Supporting information

Evaluation of accuracy of amorphous solubility advantage calculation by comparison with experimental solubility measurement in buffer and biorelevant media

Wei Zhang, [a,†] Abbe Haser,[b,†] Hao Helen Hou,[a] and Karthik Nagapudi[a,*]

[a] Small Molecule Pharmaceutical Sciences, Genentech Inc., South San Francisco, CA 94080. [b] College of Pharmacy, University of Texas-Austin, Austin, TX 78712. [†]Equal contribution. [*]Corresponding author
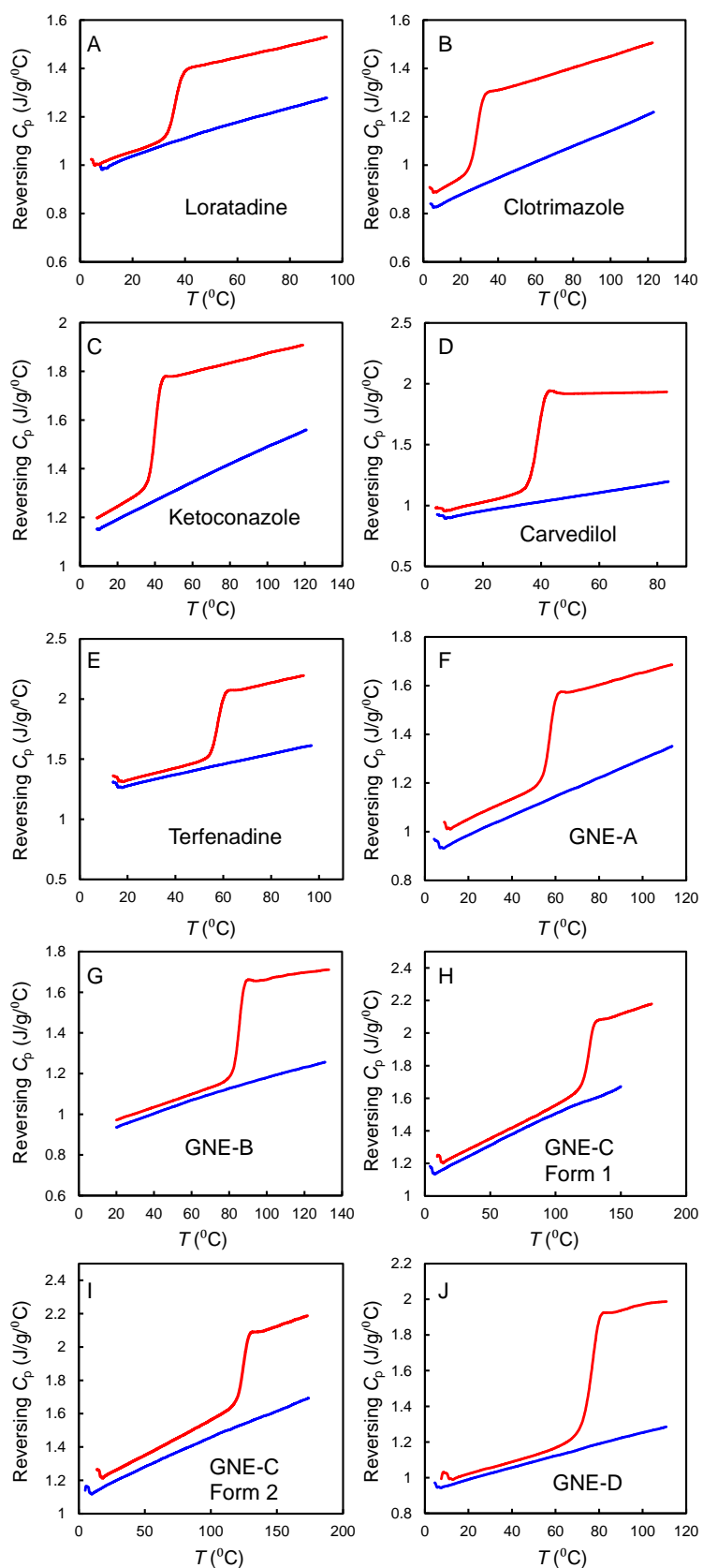
Supporting Figures

Figure S1. Heat capacity vs. temperature for all the rest systems in this work (Blue: crystal, red: supercooled liquid and amorphous solid).
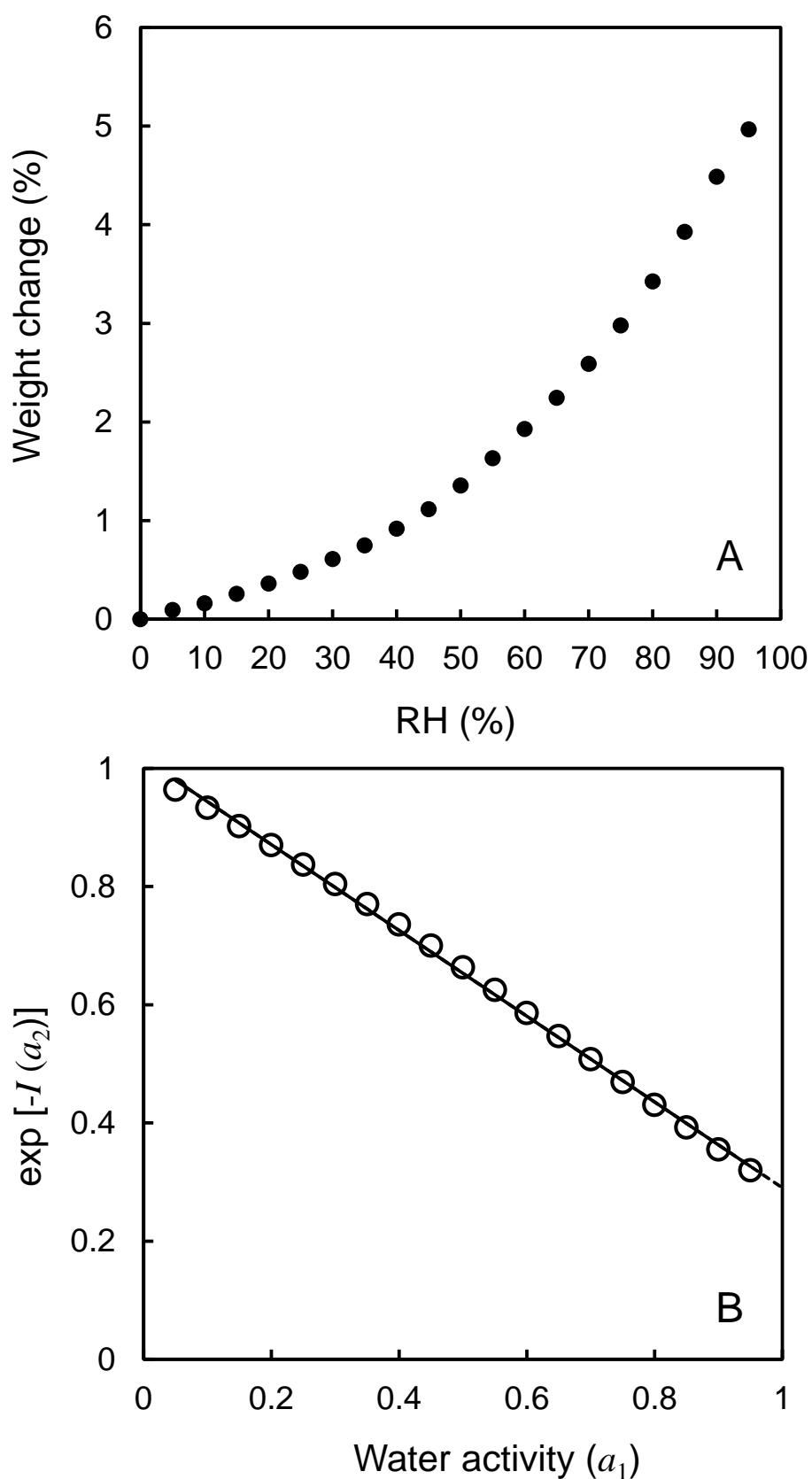
Figure S2. A. Water sorption of amorphous ritonavir measured from 0 to 95% RH by DVS. B. The exp $[-I(a_2)]$ term calculated by integration of Gibbs-Duhem equation using data from Figure S1A. Exp $[-I(a_2)]$ was extrapolated to water activity $a_1 = 1$ to represent the situation of solubility measurement in aqueous buffer. For ritonavir, exp $[-I(a_2)] = 0.29$ at water activity $a_1 = 1$.
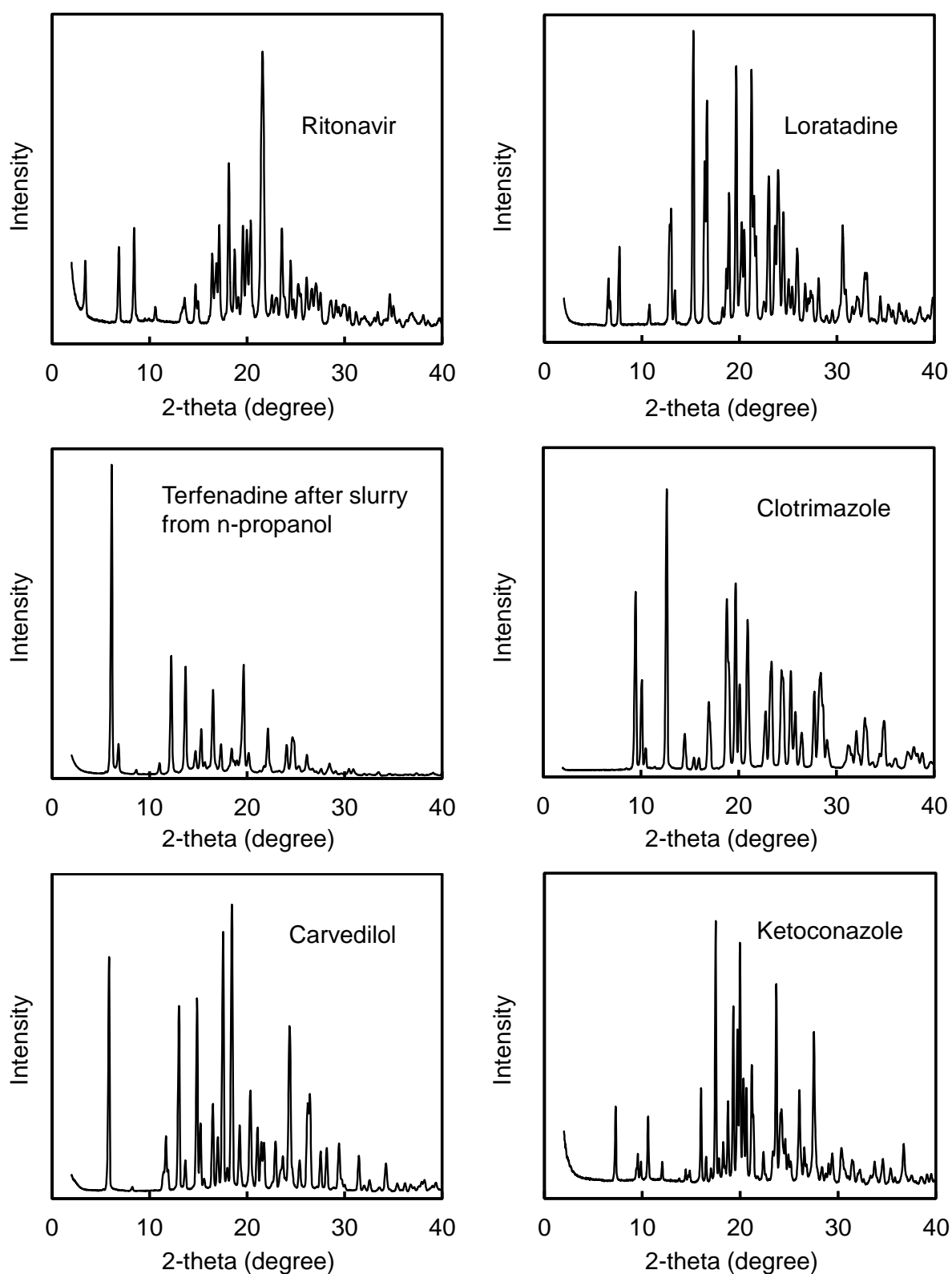
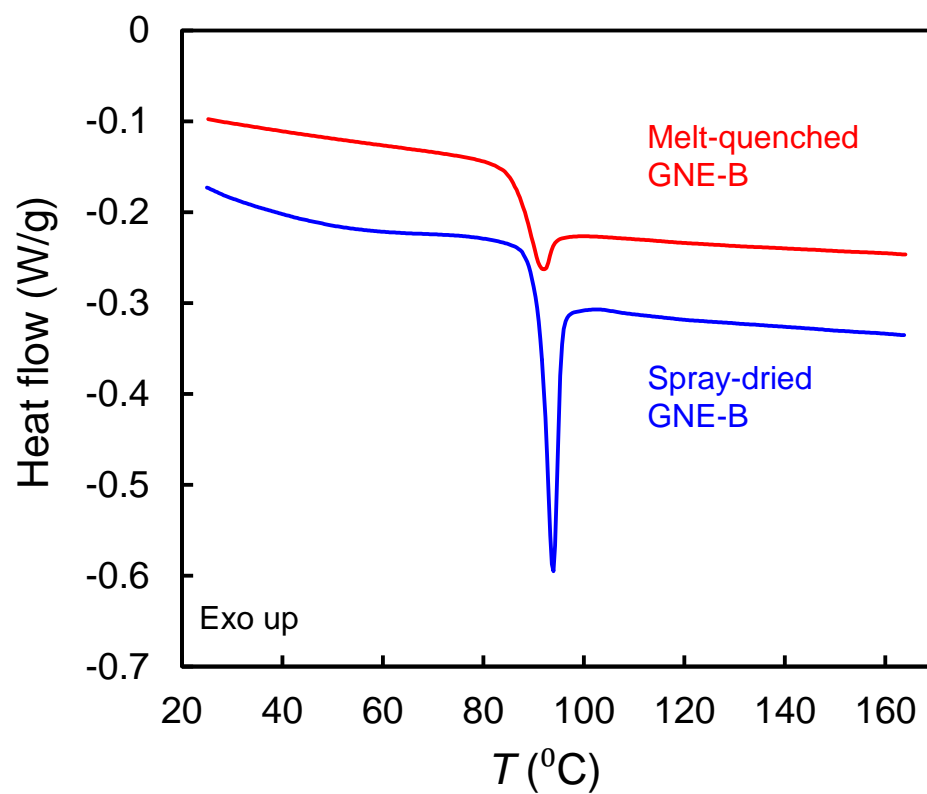Figure S3. Powder X-ray diffraction spectra for the model compounds in this study.

Figure S4. Comparison of DSC heating curves of spray-dried and melt-quenched GNE-B. The heating rate is 10 ^{0}C/min. Spray-dried sample showed a greater enthalpy relaxation and a slightly higher T_g.
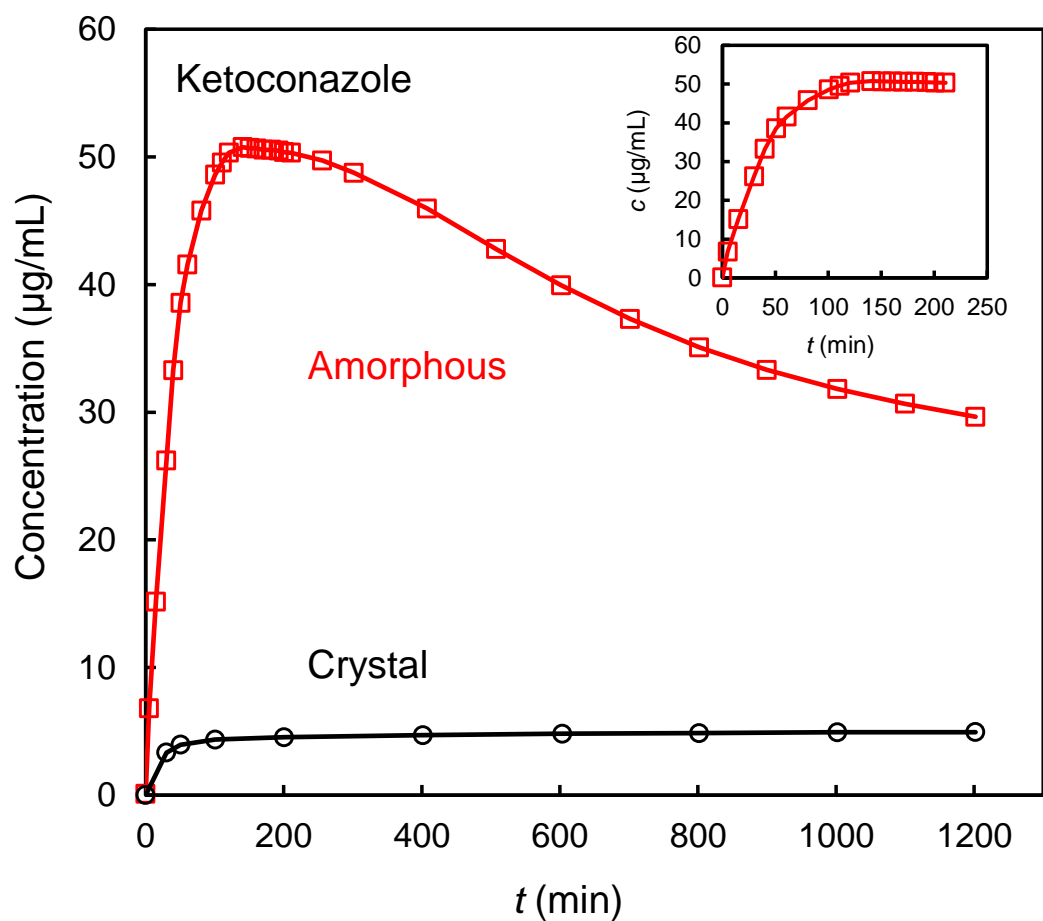
Figure S5. The dissolution profile of amorphous ketoconazole as an example to show how amorphous solubility was obtained in the case when desupersaturation occurred. The inset shows ketoconazole plateau concentration sustained for 100 min, from which amorphous solubility was determined.
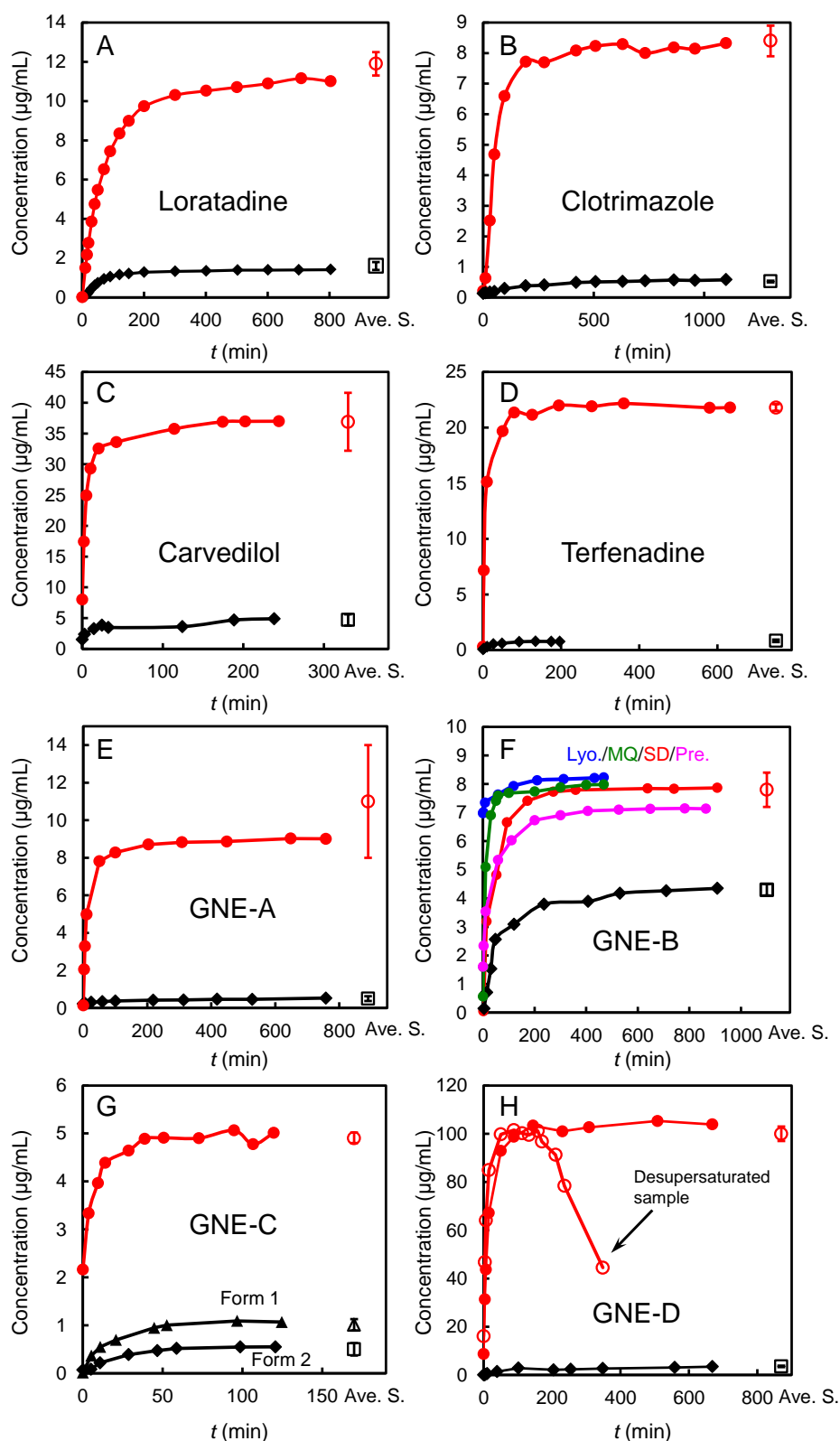
Figure S6. Typical data of amorphous and crystal solubility measurements in buffer for the rest systems. Red symbols are amorphous forms, and black symbols are crystal forms. For GNE-B, different preparation methods are labeled. For GNE-D, one sample with desupersaturation was included. The average solubilities and standard deviations from Table 4 were also included for reference. The horizontal position of a solubility point was chosen arbitrarily, not indicating the time point where concentration was taken as solubility.
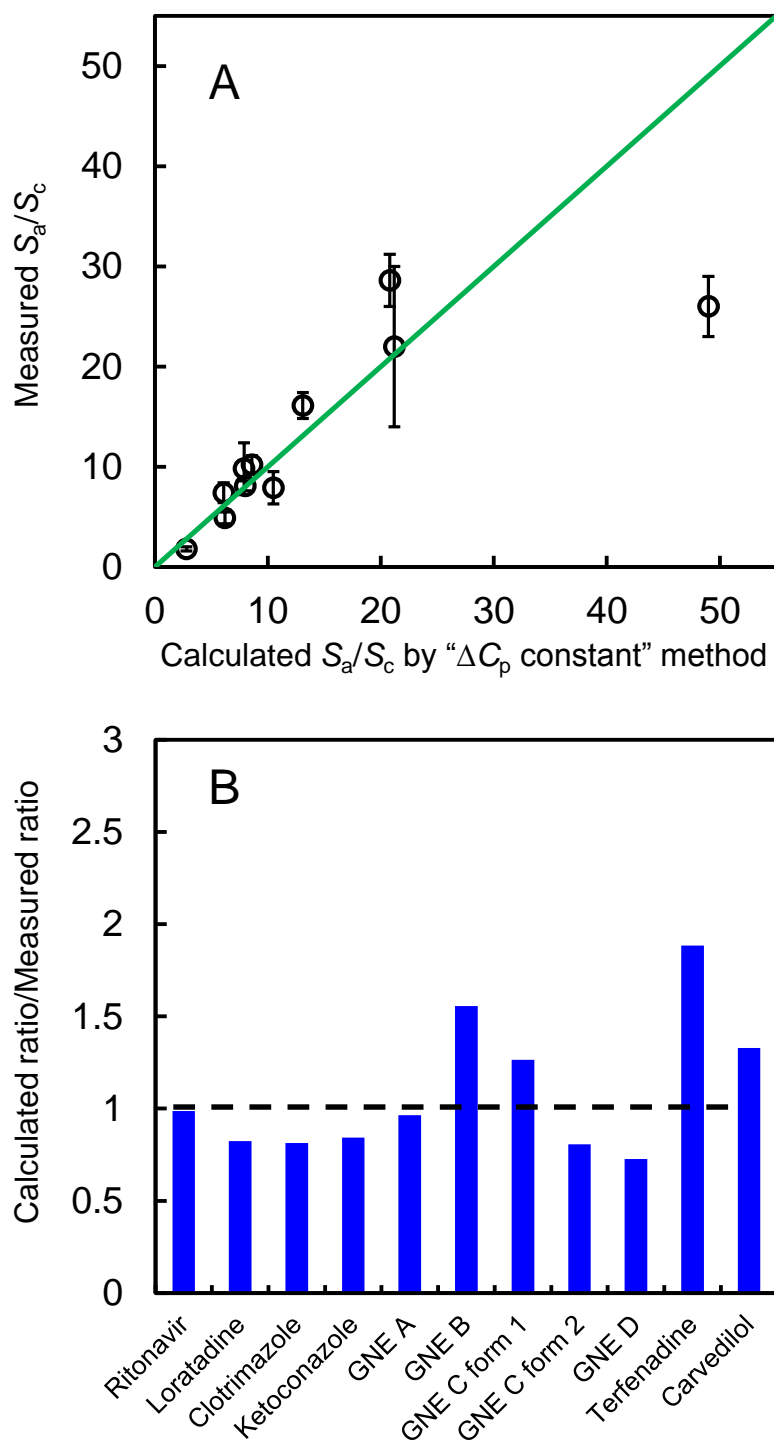
Figure S7. A. Comparison of experimentally measured amorphous solubility advantage vs. theoretical calculation by "ΔC_p constant" method. B. The ratio of calculated amorphous solubility advantage over experimentally measured amorphous solubility advantage for the ten systems.
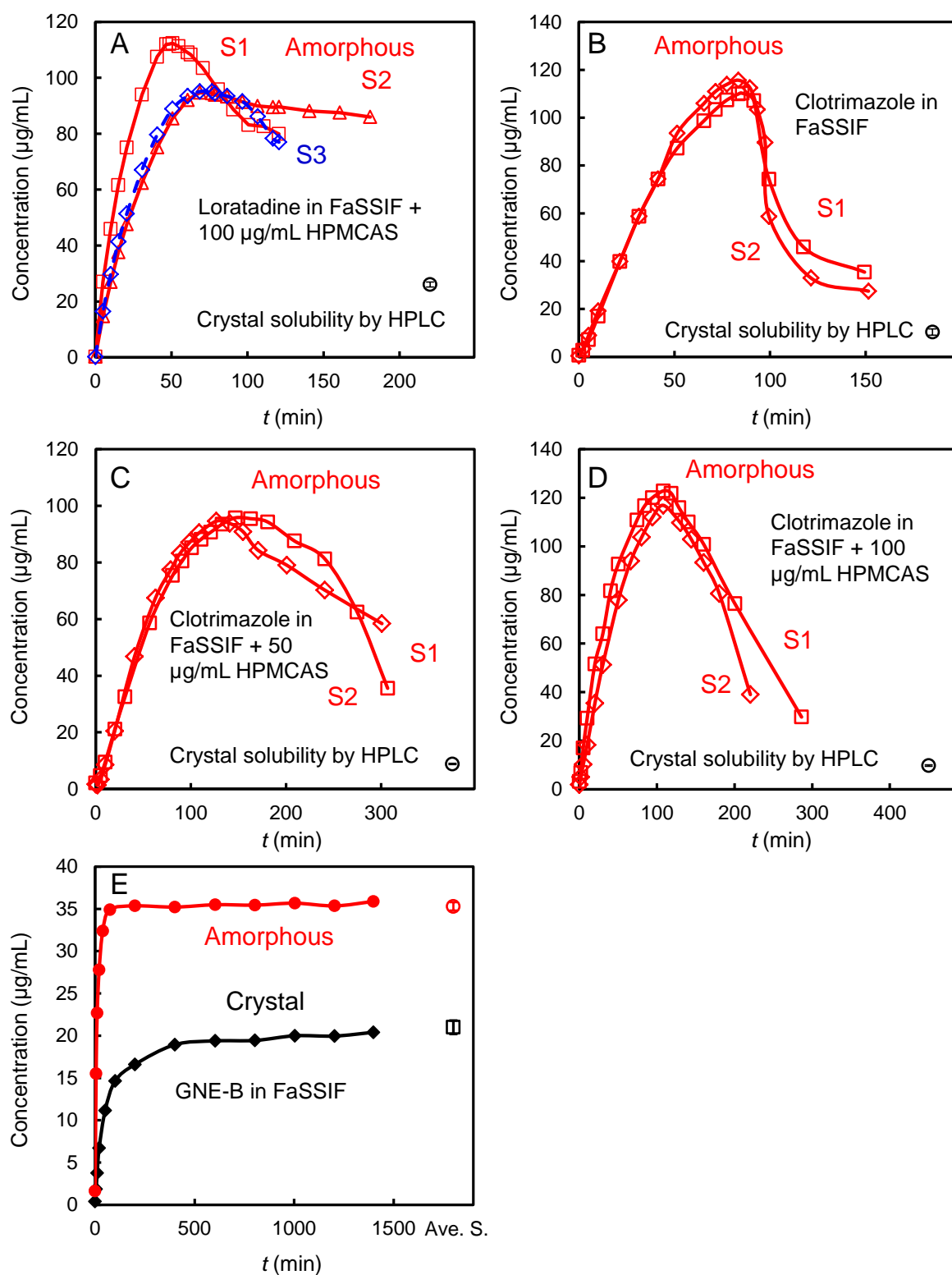
Figure S8. Dissolution and solubility measurements in FaSSIF. A. Loratadine in FaSSIF + 100 μg/mL HPMCAS. B – D. Clotrimazole in FaSSIF, FaSSIF + 50 μg/mL HPMCAS and FaSSIF + 100 μg/mL HPMCAS. Red and blue symbols are data for amorphous forms. S1, S2 and S3 refer to different samples. Black open circles represent solubilities of crystal measured in the same media by HPLC. E. GNE-B in FaSSIF. A typical data set was shown. Averaged solubility (open symbols) and standard deviation are included for reference.

Supporting Table

Table S1. Solubilities of GNE-C form 1, form 2 and amorphous form in FaSSIF measured by HPLC. The concentrations at 27 hrs were taken as solubilities and reported in Table 5.

Time/hrs	Concentration (µg/mL)		
	Form 1	Form 2	Amorphous form
22	109.2 ± 0.7	173 ± 8	960 ± 8
27	113.2 ± 0.8	173 ± 14	930 ± 17